



CHORUS

This is the accepted manuscript made available via CHORUS. The article has been published as:

Search for radiative production of the “exotic” mesons $X(3872, 3915, 3930, 3940)$ from $\psi(4160)$

T. Xiao, S. Dobbs, Kamal K. Seth, A. Tomaradze, and G. Bonvicini

Phys. Rev. D **87**, 057501 — Published 22 March 2013

DOI: [10.1103/PhysRevD.87.057501](https://doi.org/10.1103/PhysRevD.87.057501)

Search for Radiative Production of the ‘Exotic’ Mesons $X(3872, 3915, 3930, 3940)$ from $\psi(4160)$

T. Xiao,¹ S. Dobbs,¹ Kamal K. Seth,¹ A. Tomaradze,¹ and G. Bonvicini²

¹*Northwestern University, Evanston, Illinois 60208, USA*

²*Wayne State University, Detroit, Michigan 48202, USA*

(Dated: February 28, 2013)

The ‘exotic’ mesons $X(3872)$, $X(3915)$, $X(3930)$ and $X(3940)$ have been searched for in their radiative production in the $586 \text{ pb}^{-1} e^+e^-$ annihilation data taken with the CLEO-c detector at the $\psi(4160)$ resonance, and their decay in the two modes, $X \rightarrow \pi^+\pi^-J/\psi$ and $X \rightarrow \gamma J/\psi$, with $J/\psi \rightarrow \mu^+\mu^-$. No evidence for any of the four mesons is found. Upper limits for the product branching fractions, $\mathcal{B}_1(\psi(4160) \rightarrow \gamma X) \times \mathcal{B}_2(X \rightarrow \pi^+\pi^-J/\psi, \gamma J/\psi)$ have been determined. The limits at 90% confidence level range from 0.7×10^{-4} to 1.8×10^{-4} .

During the last ten years a number of unexpected hadron resonances have been reported in B-decays and e^+e^- annihilations to $J/\psi + X$. While some of them remain unconfirmed, several have been observed by both the Belle and BaBar collaborations at the KEK and SLAC B-factories [1], and at least one, $X(3872)$, has been observed in $p\bar{p}$ measurements at the Fermilab [2] and pp experiments at the LHC [3]. Because these resonances do not fit easily into the spectrum of conventional $q\bar{q}$ mesons, they are often called “exotics”, and “charmonium-like” because they invariably decay into final states which contain a charm and an anticharm quark. The masses and widths of these resonances have been measured with various levels of precision, but their J^{PC} is generally not known. While speculations abound, there is no consensus about the structures of these states. In view of this situation it is worthwhile to search for these states in alternate modes of their production and decay. In this paper we report on the search for four of these states, $X(3872)$, $X(3915)$ [4–6], $X(3930)$ [7, 8] and $X(3940)$ [9, 10], in their production in the radiative decay of $\psi(4160)$ and decay into $\pi^+\pi^-J/\psi$ and $\gamma J/\psi$.

We use 586 pb^{-1} of e^+e^- collision data taken at $\sqrt{s} = 4170 \text{ MeV}$ at the CESR collider at the Cornell University, with final state particles detected and identified in the CLEO-c detector. The CLEO-c detector has been described in detail elsewhere [11]. The detector has a cylindrically symmetric configuration, and it provides 93% coverage of solid angle for charged and neutral particle identification. The detector components important for the present measurements are the vertex drift chamber, the main drift chamber (DR), and the CsI(Tl) crystal calorimeter (CC) including end-caps.

We search for $X(3872)$, $X(3915)$, $X(3930)$ and $X(3940)$ in their radiative formation at $\sqrt{s} = 4170 \text{ MeV}$, $e^+e^- \rightarrow \gamma X$, and their decay into two final states containing J/ψ : $X \rightarrow \pi^+\pi^-J/\psi$ and $X \rightarrow \gamma J/\psi$. We reconstruct only the $J/\psi \rightarrow \mu^+\mu^-$ decay, since the $J/\psi \rightarrow e^+e^-$ decay has lower reconstruction efficiency and significantly higher QED backgrounds.

We also use CLEO-c data taken at $\psi(2S)$, $\sqrt{s} = 3686 \text{ MeV}$, for cross-checks of our analysis method in the $\gamma J/\psi$ final state by measuring the decays, $\psi(2S) \rightarrow$

$\gamma\chi_{cJ}, \chi_{cJ} \rightarrow \gamma J/\psi$. To determine our event selection criteria and reconstruction efficiencies, we use large samples of Monte Carlo (MC) simulated events.

To reconstruct the $\gamma\pi^+\pi^-J/\psi$, $J/\psi \rightarrow \mu^+\mu^-$ final state, we select events with 4 charged particle tracks with zero net charge and exactly one photon candidate. Tracks are reconstructed in the region with $|\cos\theta_{tr}| < 0.93$, where θ is the polar angle, and are required to be well-measured and consistent with originating at the interaction point. Photon candidates are calorimeter showers that are reconstructed in the “good barrel” region ($|\cos\theta_\gamma| < 0.81$) or the “good endcap” region ($0.85 < |\cos\theta_\gamma| < 0.93$) of the calorimeter, have energies larger than 50 MeV, and have a transverse energy distribution consistent with that of an electromagnetic shower.

To reconstruct the $\gamma\gamma J/\psi$, $J/\psi \rightarrow \mu^+\mu^-$ final state, we select events with two photon candidates and two oppositely charged tracks. The dominant background in this mode is from radiative QED events which peak in the forward direction ($|\cos\theta| \sim 1$), and we therefore only consider photon candidates in the “good barrel” region ($|\cos\theta_\gamma| < 0.81$) of the calorimeter, and require that they have energy of at least 100 MeV.

Charged particle tracks are first identified on the basis of their momenta. As shown in Fig. 1 (top), leptons (e, μ) from the decay of J/ψ have momenta $> 1.2 \text{ GeV}/c$, and pions have momenta $< 0.6 \text{ GeV}/c$, which makes π/μ separation easy. Pion candidates are additionally required to have an energy loss in the drift chamber (dE/dx) consistent with that expected for pions within 3σ .

Muons are distinguished from the electrons based on the variable E_{CC}/p , where p is the track momentum measured in the drift chamber and E_{CC} is the energy deposited in the calorimeter associated with the charged particle track. As shown in Fig. 1 (bottom), this variable clearly separates electrons, which deposit all of their energy in the calorimeter and have $E_{CC}/p \approx 1$, from muons which pass through the calorimeter and deposit only minimum ionizing energy. Muons are required to have $E_{CC}/p < 0.25$.

To select fully reconstructed events and improve mass resolution, a 4C kinematic fit is performed constraining the $(\pi^+\pi^-J/\psi, \gamma J/\psi) + \gamma$ final state to a common

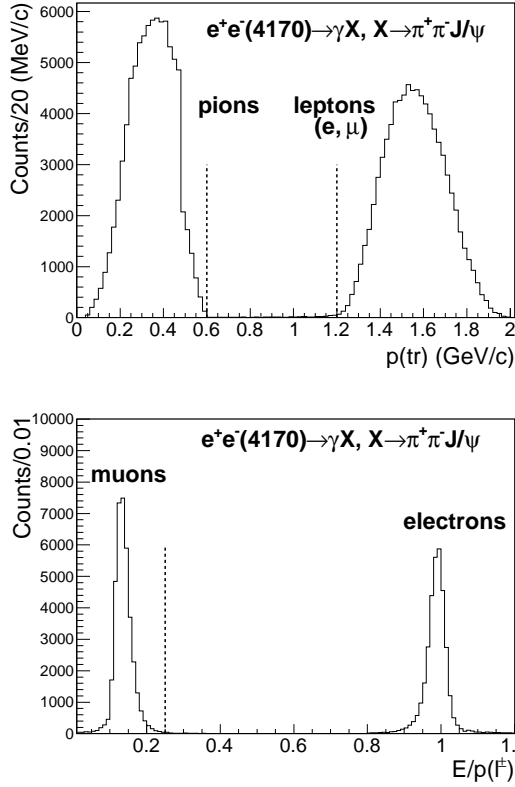


FIG. 1. Distributions of charged particle momenta (top) and E_{CC}/p (bottom) in the signal MC simulations for $e^+e^-(4170) \rightarrow \gamma X(3872)$, $X(3872) \rightarrow \pi^+\pi^- J/\psi$, $J/\psi \rightarrow \mu^+\mu^-$. Vertical dashed lines indicate the momenta cuts for pions and muons, and the E_{CC}/p cuts for muons.

vertex with $\chi^2_{\text{vertex}} < 20$, and the e^+e^- collision energy and momentum with $\chi^2_{4C \text{ fit}} < 20$. In the following, we use the momenta of the charged particles and photons after the kinematic fit. To select events containing a $J/\psi \rightarrow \mu^+\mu^-$ decay, we select events with a dimuon mass consistent with that of the J/ψ within $\pm 30 \text{ MeV}/c^2$. Fig. 2 shows the $\mu^+\mu^-$ invariant mass distributions in both $X \rightarrow \pi^+\pi^- J/\psi$ and $X \rightarrow \gamma J/\psi$ channels. The MC generated, arbitrarily normalized J/ψ peak is superposed on the data distributions. The J/ψ peak is prominently visible in the $X \rightarrow \pi^+\pi^- J/\psi$ decay (primarily due to the prolific decay $\psi(2S) \rightarrow \pi^+\pi^- J/\psi$, with $\psi(2S)$ formed by initial state radiation (ISR)). The J/ψ peak in the decay $X \rightarrow \gamma J/\psi$ is seen only as a small enhancement over the background.

Fig. 3 shows the mass distributions for both final states after all event selections have been applied. In the $\pi^+\pi^- J/\psi$ final state (Fig. 3(left)) a strong peak corresponding to the ISR excitation of the $\psi(2S)$ is clearly visible, while no signal is apparent in the $> 3.75 \text{ GeV}/c^2$ region. In the $\gamma J/\psi$ final state (Fig. 3(right)), no structures above the background are seen.

In order to validate our event selection criteria for the

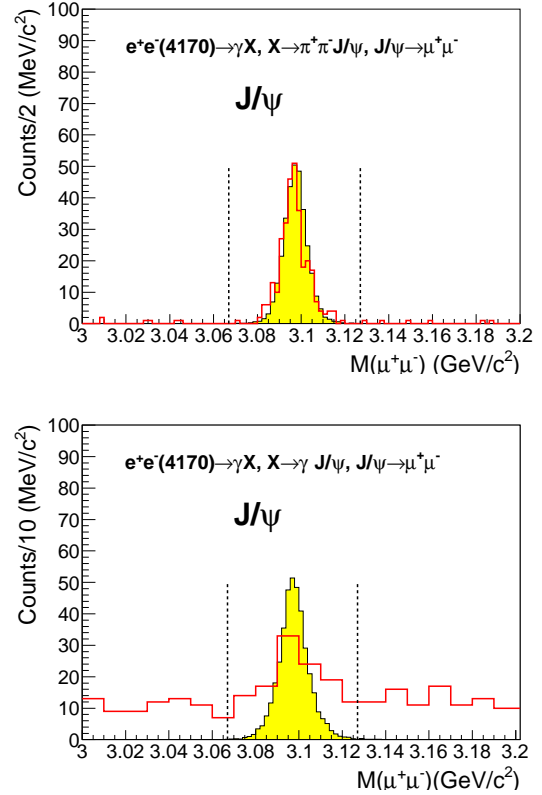


FIG. 2. J/ψ invariant mass distributions after kinematic fit in data (red solid histogram) and the $X(3872)$ signal MC (shaded histograms). Top: $X \rightarrow \pi^+\pi^- J/\psi$ channel; Bottom: $X \rightarrow \gamma J/\psi$ channel.

$\pi^+\pi^- J/\psi$ final state, we use the observed $\psi(2S)$ ISR peak to derive $\mathcal{B}(\psi(2S) \rightarrow \pi^+\pi^- J/\psi)$, and compare it with its known value from the PDG(2012) [12]. For the $\gamma J/\psi$ final state, we analyze the CLEO-c data for 24.5 million $\psi(2S)$ to determine the product $\mathcal{B}(\psi(2S) \rightarrow \gamma\chi_{c1,2}) \times \mathcal{B}(\chi_{c1,2} \rightarrow \gamma J/\psi)$ and compare it with the published CLEO results [13]. For both decays the results agree with the known values within their statistical uncertainties.

Since no evidence for any X resonance is seen in either spectra shown in Fig. 3, we set upper and lower limits for their production using the Feldman-Cousins method to derive confidence limits [14]. We take the expected signal region to be $\pm \Gamma_{\text{exp}}$ around the known X masses, where the expected signal width Γ_{exp} is determined by convoluting the known Breit-Wigner width of X and the detector resolution width of $12.2 \text{ MeV}/c^2$ for the $\pi^+\pi^- J/\psi$ final state, and of $15.5 \text{ MeV}/c^2$ for the $\gamma J/\psi$ final state, as determined by MC simulations. Table I summarizes the world-average resonance parameters of the X states [12], the expected signal widths Γ_{exp} , and the resulting signal regions, defined as $M(X) \pm \Gamma_{\text{exp}}(X)$. As shown in Fig. 3, the backgrounds in both spectra are found to be constant, with an average of 0.22 events/5 (MeV/c^2) bin

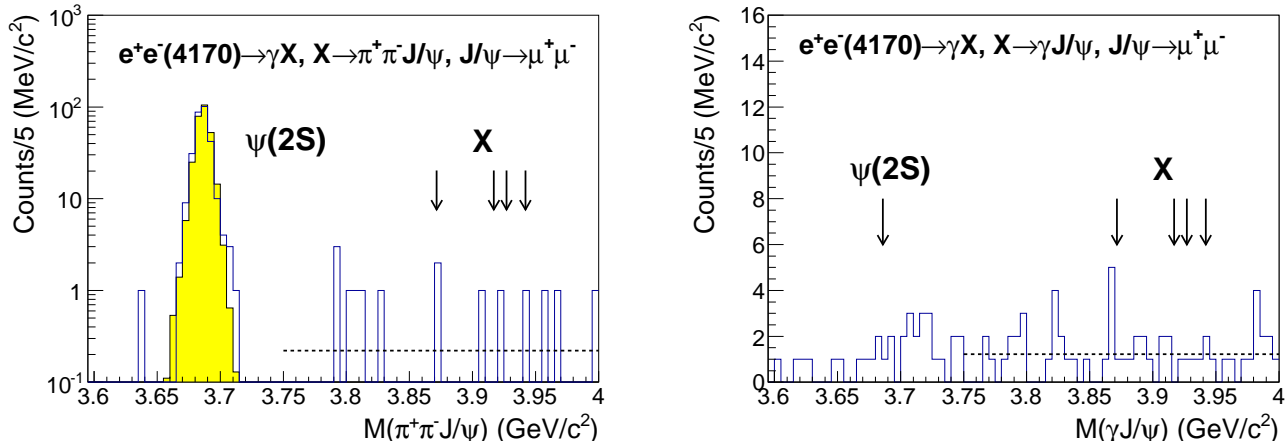


FIG. 3. Invariant mass distributions of (left) $M(\pi^+\pi^-J/\psi)$ and (right) $M(\gamma J/\psi)$ for the data taken at $\sqrt{s} = 4170$ MeV. The shaded histogram in the left panel shows the arbitrarily scaled ISR excitation of $\psi(2S)$ from MC simulation. The arrows labeled “X” indicate the peak locations of the X states given in Table I. The dashed lines show the constant backgrounds in the > 3.75 GeV/c^2 regions of both spectra.

TABLE I. Summary of the world-average resonance mass M and width Γ_{BW} for the X states from PDG [12], the expected signal width Γ_{exp} , and the signal region $M(X) \pm \Gamma_{\text{exp}}(X)$ for each X state.

state	M (MeV/c^2)	Γ_{BW} (MeV/c^2)	Γ_{exp} (MeV/c^2)		signal region (MeV/c^2)	
			$\pi^+\pi^-J/\psi$	$\gamma J/\psi$	$\pi^+\pi^-J/\psi$	$\gamma J/\psi$
X(3872)	3871.68 ± 0.17	< 1.2	13.4	16.7	3872 ± 13	3872 ± 17
X(3915)	3917.5 ± 2.7	27 ± 10	39.2	42.5	3918 ± 39	3918 ± 43
X(3930)	3927.2 ± 2.6	24 ± 6	36.2	39.5	3927 ± 36	3927 ± 40
X(3940)	3942_{-8}^{+9}	37_{-17}^{+27}	49.2	52.5	3942 ± 49	3942 ± 53

for the $\pi^+\pi^-J/\psi$ final state, and 1.22 events/5 (MeV/c^2) bin for the $\gamma J/\psi$ final state. In Table II we list the MC determined efficiencies, the total number of counts N_{obs} in the signal region, and the estimated number of background counts N_{bkg} in that region. Using the method of Feldman and Cousins, the upper and lower limits on signal counts at the 90% confidence level are obtained. The lower limits in all cases are zero. The upper limits N_{UL} are listed in Table II.

The corresponding upper limits on the branching fractions for $\mathcal{B}_1(\psi(4160) \rightarrow \gamma X) \times \mathcal{B}_2(X \rightarrow \pi^+\pi^-J/\psi, \gamma J/\psi)$ are calculated as:

$$\mathcal{B}_1 \times \mathcal{B}_2 = \frac{N_{\text{UL}}}{\epsilon \times \mathcal{L} \times \sigma_{\psi(4160)} \times \mathcal{B}(J/\psi \rightarrow \mu^+\mu^-)} \quad (1)$$

where $\mathcal{B}_1 \equiv \mathcal{B}_1(\psi(4160) \rightarrow \gamma X)$, $\mathcal{B}_2 \equiv \mathcal{B}_2(X \rightarrow \pi^+\pi^-J/\psi, \gamma J/\psi)$, N_{UL} is the upper limit on the number of signal events at the 90% confidence level, ϵ is the MC-determined efficiency, $\mathcal{L}(= 586 \text{ pb}^{-1})$ is the e^+e^- luminosity, $\sigma_{\psi(4160)}(= 9.45 \pm 0.50 \text{ nb})$ is the total hadronic cross section at $\sqrt{s} = 4170$ MeV, which we assign fully to the $\psi(4160)$ resonance [15], and $\mathcal{B}(J/\psi \rightarrow \mu^+\mu^-) = 5.93\%$ [12].

We estimate the systematic uncertainties due to track and photon reconstruction to be 1% per track and 2% per photon. We estimate a 1% uncertainty due to the luminosity measurement [16]. We vary the MC-determined resolution widths by $\pm 10\%$. We also vary the assumed values of mass and width for the X states by their uncertainties in the average values given in Table I. Taking account of these systematic uncertainties we obtain the upper limits in the last column of Table II.

For X(3872) our results for product branching fractions can be compared with those obtained by Belle and BaBar from radiative decay of $\Upsilon(2S)$, and from $B^{\pm,0}$ decays. Table III lists these results.

The X(3930) state was assigned $J^{PC} = 2^{++}$ by Belle [22], and is considered to be a good candidate for $\chi'_{c2}(2^3P_2)$. With this identification, and the identification of the 4160 MeV/c^2 resonance as $\psi(2^3D_2)$, according to the non-relativistic calculation of Barnes, Godfrey and Swanson [23], the expected product branching fraction $\mathcal{B}(\psi(2^3D_2) \rightarrow \gamma \chi'_{c2}(2^3P_2)) \times \mathcal{B}(\chi'_{c2}(2^3P_2) \rightarrow \gamma J/\psi) = 8 \times 10^{-8}$. Similarly, if X(3872) is assigned $J^{PC} = 1^{++}$ and identified as $\chi'_{c1}(2^3P_1)$, their prediction is $\mathcal{B}(\psi(2^3D_2) \rightarrow \gamma \chi'_{c1}(2^3P_1)) \times \mathcal{B}(\chi'_{c1}(2^3P_1) \rightarrow \gamma J/\psi) = 1.7 \times 10^{-6}$.

TABLE II. Results of the 90% confidence level upper limits for the product branching fractions, $\mathcal{B}_1 \times \mathcal{B}_2 \equiv \mathcal{B}_1(\psi(4160) \rightarrow \gamma X) \times \mathcal{B}_2(X \rightarrow \pi^+ \pi^- J/\psi, \gamma J/\psi)$, as described in the text. N_{obs} and N_{bkg} are the number of observed and estimated background counts in each signal region, N_{UL} is the 90% confidence level upper limit for counts as described in the text, and ϵ is the MC-determined efficiency.

channel	state	$\epsilon(\%)$	signal region (MeV/c^2)	N_{obs}	N_{bkg}	N_{UL}	$\mathcal{B}_1 \times \mathcal{B}_2 \times 10^4$
$\pi^+ \pi^- J/\psi$	$X(3872)$	24.6	3872 ± 13	2	1.1	< 4.8	< 0.68
	$X(3915)$	20.0	3918 ± 39	3	3.3	< 4.1	< 1.36
	$X(3930)$	18.0	3927 ± 36	4	3.3	< 5.3	< 1.18
	$X(3940)$	16.9	3942 ± 49	5	4.2	< 5.8	< 1.47
$\gamma J/\psi$	$X(3872)$	29.9	3872 ± 17	11	8.5	< 9.3	< 1.05
	$X(3915)$	30.4	3918 ± 43	20	20.7	< 7.8	< 1.26
	$X(3930)$	30.1	3927 ± 40	18	18.3	< 7.9	< 0.88
	$X(3940)$	29.7	3942 ± 53	28	25.6	< 12.4	< 1.79

TABLE III. Comparison of our product branching fraction results with the recent measurements from Belle and BaBar. For clarity we abbreviate $X(3872)$ to just X in this table. The upper limits are at 90% confidence level.

Experiment	Branching Fraction	Value
Present	$\mathcal{B}_1(\psi(4160) \rightarrow \gamma X) \times \mathcal{B}_2(X \rightarrow \pi^+ \pi^- J/\psi)$	$< 6.8 \times 10^{-5}$
Belle [17]	$\mathcal{B}(\Upsilon(2S) \rightarrow \gamma X) \times \mathcal{B}(X \rightarrow \pi^+ \pi^- J/\psi)$	$< 0.8 \times 10^{-6}$
BaBar [18]/Belle [19]	$\mathcal{B}(B^+ \rightarrow XK^+) \times \mathcal{B}(X \rightarrow \pi^+ \pi^- J/\psi)$	$= (8.4 \pm 1.7) \times 10^{-6} / (8.6 \pm 1.0) \times 10^{-6}$
	$\mathcal{B}(B^0 \rightarrow XK^0) \times \mathcal{B}(X \rightarrow \pi^+ \pi^- J/\psi)$	$= (3.5 \pm 1.9) \times 10^{-6} / (4.3 \pm 1.3) \times 10^{-6}$
Present	$\mathcal{B}_1(\psi(4160) \rightarrow \gamma X) \times \mathcal{B}_2(X \rightarrow \gamma J/\psi)$	$< 1.05 \times 10^{-4}$
BaBar [20]/Belle [21]	$\mathcal{B}(B^\pm \rightarrow XK^\pm) \times \mathcal{B}(X \rightarrow \gamma J/\psi)$	$= (2.8 \pm 0.8) \times 10^{-6} / (1.78_{-0.46}^{+0.49}) \times 10^{-6}$

To summarize, we find no significant signals for the $X(3872)$, $X(3915)$, $X(3930)$, or $X(3940)$ in $\psi(4160)$ radiative decays and we set upper limits on $\mathcal{B}_1(\psi(4160) \rightarrow \gamma X) \times \mathcal{B}_2(X \rightarrow \pi^+ \pi^- J/\psi, \gamma J/\psi)$, which range from 0.7×10^{-4} to 1.8×10^{-4} at 90% confidence level. In order to indicate the general level of sensitivity of our data and the analysis method, we estimate upper limits for any resonance X with a mass in the range of $3750 \text{ MeV}/c^2$ to $4000 \text{ MeV}/c^2$, and an expected signal width of $40 \text{ MeV}/c^2$ for $X \rightarrow \pi^+ \pi^- J/\psi$ decay and $45 \text{ MeV}/c^2$ for $X \rightarrow \gamma J/\psi$ decay. The efficiency is assumed to be 20% for $X \rightarrow \pi^+ \pi^- J/\psi$ decay and 30% for $X \rightarrow \gamma J/\psi$ decay. The systematic uncertainties due to track and photon reconstruction and the luminosity measurement are taken into account. Fig. 4 shows the 90% confidence level upper limits on $\mathcal{B}_1(\psi(4160) \rightarrow \gamma X) \times \mathcal{B}_2(X \rightarrow \pi^+ \pi^- J/\psi, \gamma J/\psi)$ for X as functions of $M(X)$ in $10 \text{ MeV}/c^2$ steps.

This investigation was done using CLEO data, and as members of the former CLEO Collaboration we thank it for this privilege. This research was supported by the U.S. Department of Energy.

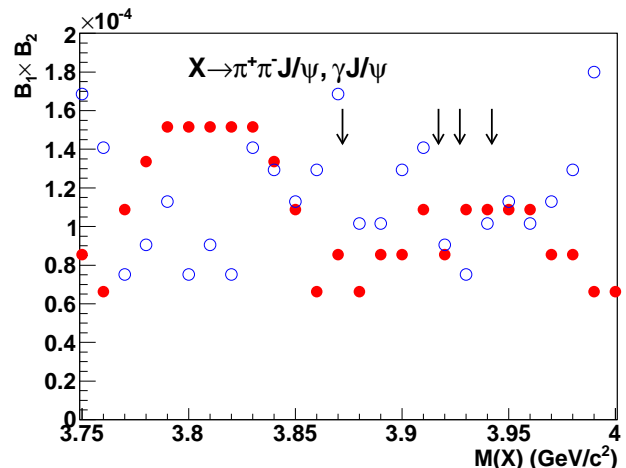


FIG. 4. 90% confidence level upper limits for $\mathcal{B}_1 \times \mathcal{B}_2$, $\mathcal{B}_1 \equiv \mathcal{B}_1(\psi(4160) \rightarrow \gamma X)$, $\mathcal{B}_2 \equiv \mathcal{B}_2(X \rightarrow \pi^+ \pi^- J/\psi)$ (solid points) and $\mathcal{B}_2(X \rightarrow \gamma J/\psi)$ (open points). The arrows indicate the peak locations of the $X(3872)$, $X(3915)$, $X(3930)$ and $X(3940)$ states.

-
- [1] For reviews see, for example, E. S. Swanson, Phys. Rep. **429**, 243 (2006); N. Brambilla *et al.*, Eur. Phys. J. C **71**, 1534 (2011); Kamal K. Seth, Prog. Part. Nucl. Phys. **67**, 390 (2012).
- [2] D. Acosta *et al.* [CDF II Collaboration], Phys. Rev. Lett. **93**, 072001 (2004).
- [3] The LHCb Collaboration, [arXiv:1112.5310](https://arxiv.org/abs/1112.5310) [hep-ex].
- [4] S. K. Choi *et al.* [Belle Collaboration], Phys. Rev. Lett. **94**, 182002 (2005).
- [5] B. Aubert *et al.* [BaBar Collaboration], Phys. Rev. Lett. **101**, 082001 (2008).
- [6] S. K. Choi *et al.* [Belle Collaboration], Phys. Rev. Lett. **104**, 092001 (2010).
- [7] B. Aubert *et al.* [BaBar Collaboration], Phys. Rev. D **81**, 092003 (2010).
- [8] S. Uehara *et al.* [Belle Collaboration], Phys. Rev. Lett. **96**, 082003 (2006).
- [9] K. Abe *et al.* [Belle Collaboration], Phys. Rev. Lett. **98**, 082001 (2007).
- [10] P. Pakhlov *et al.* [Belle Collaboration], Phys. Rev. Lett. **100**, 202001 (2008).
- [11] Y. Kubota *et al.* [CLEO Collaboration], Nucl. Instrum. Meth. A **320**, 66 (1992); M. Artuso *et al.*, Nucl. Instrum. Meth. A **554**, 147 (2005); D. Peterson *et al.*, Nucl. Instrum. Meth. A **478**, 142 (2002).
- [12] J. Beringer *et al.* [Particle Data Group], Phys. Rev. D **86**, 010001 (2012).
- [13] H. Mendez *et al.* [CLEO Collaboration], Phys. Rev. D **78**, 011102 (2008).
- [14] G. J. Feldman and R. D. Cousins, Phys. Rev. D **57**, 3873 (1998).
- [15] D. Cronin-Hennessy *et al.* [CLEO Collaboration], Phys. Rev. D **80**, 072001 (2009).
- [16] S. Dobbs *et al.* [CLEO Collaboration], Phys. Rev. D **76**, 112001 (2007).
- [17] X. L. Wang *et al.* [Belle Collaboration], Phys. Rev. D **84**, 071107(R) (2011).
- [18] B. Aubert *et al.* [BaBar Collaboration], Phys. Rev. D **77**, 111101(R) (2008).
- [19] S. K. Choi *et al.* [Belle Collaboration], Phys. Rev. D **84**, 052004 (2011).
- [20] B. Aubert *et al.* [BaBar Collaboration], Phys. Rev. Lett. **102**, 132001 (2009).
- [21] V. Bhardwaj *et al.* [Belle Collaboration], Phys. Rev. Lett. **107**, 091803 (2011).
- [22] S. Uehara *et al.* [Belle Collaboration], Phys. Rev. Lett. **96**, 082003 (2006).
- [23] T. Barnes, S. Godfrey, and E. S. Swanson, Phys. Rev. D **72**, 054026 (2005).